Quantitative infrared thermography in thermo-fluid-dynamics

by G. Cardone

Università degli Studi di Napoli "Federico II", Dipartimento di Energetica, Termofluidodinamica Applicata e Condizionamenti Ambientali (DETEC) P.le Tecchio 80, 80 125 Napoli, ITALY

Abstract

Infrared (IR) thermography, due to its two-dimensionality and non-contact character, can be usefully employed in a vast variety of heat transfer industrial applications as well as research fields. The present work deals with measurements of temperature and/or convective heat transfer coefficients in two types of fluid flow configurations (internal and external) studied by means of the IR scanning radiometer applied to the *heated-thin-foil* technique. In more details, it is analysed the capability of the infrared system to study particular phenomena such as: the heat transfer in a static 180deg turn channel and heat transfer to air from a yawed circular cylinder.

1. Introduction

Measurement of heat flux rates and/or convective heat transfer coefficients from a surface to a stream is more difficult to perform than other common thermo-fluid-dynamic quantities. Usually, measuring heat fluxes involves measuring temperatures. In the ordinary techniques, where the temperature is measured by thermocouples, resistance temperature detectors (RTDs), or pyrometers, the sensor yields the local heat flux at a single point (or the space-averaged one); hence, the sensor itself can be considered as zero-dimensional. This limitation makes experimental work particularly troublesome whenever temperature and/or heat flux fields exhibit high spatial gradients.

The IRSR can be regarded as a true two-dimensional temperature sensor since it allows accurate measurements of surface temperature maps also in presence of high spatial temperature, and/or heat-flux, gradients; its spatial resolution mainly depends on the camera and on the employed optics. The IR system generally measures the object skin temperatures and so it can be also regarded as a thin-film sensor or, better, as a two-dimensional array of thin films; however, the response time of IRSR is typically of the order of 10^{-1}-10^{-2} s.

Heat-flux sensors generally consist of slabs with a known thermal behaviour, whose temperature is measured at fixed points (Carlomagno et al. [1]). The equation for heat conduction in solids applied to a proper sensor model yields the relationship by which the measured temperature is correlated to the convective heat transfer rate.

The use of IRSR as a temperature sensor in convective heat transfer measurements appears advantageous, from several points of view, compared to standard sensors. In fact, as already mentioned, IRSR is a fully two-dimensional sensor; it allows the evaluation of errors due to tangential conduction and radiation, and it is noninvasive. This last characteristic also eliminates the conduction errors through the thermocouple's or RTD's wires. The accuracy of a measurement depends on the knowledge of the emissivity coefficient of the surface viewed by an IR camera; however, an error in the evaluation of the emissivity coefficient leads to a smaller error in the temperature measurement.

As illustrated by Carlomagno [2], the use of a fully computerized infrared imaging system matches both qualitative and quantitative requirements. In certain applications, as in shock tunnels (Simeonides et al. [3], Henckels et al. [4]), or when dealing with moving objects (Cardone et al. [5]), the so-called *line-scan* option (consisting of locking the *vertical* scanning mechanism of the radiometer) may be used to respectively decrease the response time, or to reconstruct the thermal image. Of course, in the *line-scan* mode, unless the object is moving, the measurement is intrinsically one-dimensional.

The experimental procedure to be considered, for the measurement of convective heat transfer coefficients, depends on the particular Mach number range M of the flow. In the case of an iposonic flow regime (M<<1) the aerodynamic heating is not adequate for the IRSR sensitivity, so it is necessary to create a temperature difference between the model surface and the flow, i.e. it is necessary to transfer heat to the model in the so-called *active* mode. This may be attained either by varying the flow temperature (e.g., by heating the stream or, in some cases, by turning off the cooling device of a wind tunnel facility), or by heating the model in steady or transient ways. Models of cylindrical geometry (e.g. 2D airfoils, pipes, plates etc.) can be easily heated by Joule effect if their surface is made of a very thin metallic foil or of a thin printed circuit board. In such cases the convective heat transfer coefficient from the model surface to the flowing stream is measured by the so-called *heated-thin-foil* technique. By applying this technique Carlomagno et al.[6] studied the heat transfer from a plate to impinging jets; de Luca et al. [7] characterise the boundary layer development over a model wing to detect transition and separation regions; Cardone et al. [8] analyse steady state and transient natural convection over a vertical plate. Conversely, the model can be heated by means of a radiative source whose effects are superimposed to the convective ones. Heath et al. [9] monitor, with a line-scan utilization of IRSR, the temperature decay when the heating, from a CO_2 laser scan, ceases. Balageas et al. [10] propose two methods of inferring the heat transfer coefficient from the measured temperature, one based on the zero order time moment of temperature and the other one by using the temperature Laplace transform.

At high Mach numbers, because of the stream high kinetic energy content, the detection of the thermal image may be obtained by the so-called *passive* mode. The model, initially at uniform ambient temperature, is suddenly exposed to the high total temperature air stream; according to the properly selected thermal model, the *thin-skin* (e.g. Carlomagno et al. [11]) or the *thin-film* (e.g. Bynum et al. [12], de Luca et al. [13]) techniques are used to obtain the convective heat transfer coefficients and/or to investigate the boundary layer behaviour.

The possibility that measurements of convective heat transfer coefficients may be performed accurately by means of an IR imaging system depends on the possibility that all the potential error sources linked to the object, the environment and the acquisition system may be eliminated.

Generally, a heat flux harmonically varying (in one direction) over a surface should theoretically cause a corresponding harmonic temperature distribution. In any case, the heat flux sensor is never perfectly one dimensional, i.e. adiabatic along the direction parallel to the surface (tangential direction). Therefore, some thermal conduction in the tangential direction exists within the sensor so that the temperature distribution is modulated with a corresponding decrease of the temperature amplitude. An additional modulation can be caused by the radiative heat transfer from the surface to the ambient. This modulation will maintain a harmonic temperature distribution only for relatively small temperature differences when a linearization can be applied.

Mainly due to the finite dimensions of the IR temperature sensor, another modulation is introduced by the *Modulation Transfer Function* (*MTF*) of the camera that produces a signal of decreasing amplitude for increasing spatial frequency. Moreover, a further decrease of the temperature amplitude may be introduced by the analog-to-digital (A/D) converter when sampling the analog signal in single detector cameras.

All the above effects therefore reduce, to a greater or a lower extent, the temperature amplitude according to the experimental conditions as well as to the measuring device and evidence the need of restoration of the thermal image. Carlomagno [14] report a detailed analysis of involved errors and the relative restoration procedure.

The attention of the present work is focused on the measurement of convective heat transfer coefficients performed by means of infrared thermography applied to the *heated-thin-foil* technique. The capability of IR thermography to characterize the thermal behaviour of the flow in two different fluid configurations is highlighted. In particular: the heat transfer in a static 180deg turn channel and the heat transfer to air from a yawed circular cylinder.

2. *Heated-thin-foil* data reduction

The *heated-thin-foil* method consists of heating a thin metallic foil by Joule effect and computing the convective heat transfer coefficient h from the foil to the stream flowing on it, by means of the relationship:

$$h = \frac{\dot{q}_j - \dot{q}_1}{T_w - T_{aw}} \tag{1}$$

where: $\dot{q}_j$ is the known Joule heating; $\dot{q}_l$ includes the thermal losses mainly due to tangential conduction $\dot{q}_c$ and radiation $\dot{q}_r$, T_w is the wall temperature which is measured when heating the foil (hot image) and T_{aw} is the adiabatic wall temperature (without heating, cold image). The foil is generally thermally insulated at its backface, i.e. the face opposite to that the stream is flowing over. When this insulation cannot be accomplished, e.g. for optical access reasons, additional thermal losses, such as natural convection and radiation, must be taken into account. Generally, the measurement can be performed on both sides of the foil; in fact, if the Biot number $Bi = hb/\kappa$ (where κ and b are the foil thermal conductivity and thickness, respectively) is relatively small, the foil can be considered isothermal across its thickness.

The tangential conduction $\dot{q}_c$, which modulates the thermal signal, may be evaluated by means of the second derivative of the wall temperature T_w. The evaluation of the second derivative of T_w is eased by the fact that IRSR yields a very large number of wall temperatures. However, it has to be pointed out that spurious effects linked to the noise have to be avoided by filtering the temperature signal; in the steady state *heated-thin-foil* technique, the noise can be also strongly reduced by averaging a large number of thermal images acquired in a time sequence. When the *heated-thin-foil* is made of a printed circuit board, the bulk tangential conduction behaviour of the foil may be non isotropic.

The losses due to radiation $\dot{q}_r$ may be evaluated according to radiative net flux law (derived from the radiosity concept when the surrounding is very large with respect to the target or if the surrounding is considered a black body):

$$\dot{q}_r = \varepsilon\sigma\left(T_w^4 - T_a^4\right) \tag{2}$$

where ε is the total emissivity coefficient, σ is the Stefan-Boltzman constant and T_a is the ambient temperature. Under the assumption that the spectral emissivity coefficient ε_λ does not vary much, the total emissivity coefficient ε of the surface under test may be measured by the IR termography itself by relating the detected radiation from a specimen heated by means of a bath/circulator with its actual temperature monitored by a precise thermometer.

The infrared radiation measured by an IR system can be also affected by atmospheric damping and includes reflected radiation from object surroundings; these factors may be taken into account by calibration and correction procedures.

3. Heat transfer measurements in a static 180deg turn channel

The thermal efficiency of gas turbine engines strongly depends on the gas entry temperature; the higher this temperature, the more efficient is the turbine thermal cycle. Present advanced gas turbines operate at gas entry temperatures much higher than metal creeping temperatures and therefore require intensive cooling of their blades especially in the first stages. A way of cooling turbine blades is by means of internal forced convection: generally, cooling air from the compressor is supplied through the hub section into the blade interior and, after flowing through a serpentine passage, is discharged at the blade trailing edge. The serpentine passage is mostly made of several adjacent straight ducts, spanwise aligned, which are connected by 180deg turns. The presence of these turns causes flow separation and reattachment and induces secondary flows; the overall effect is that the

convective heat transfer coefficient exhibits an increase associated with high local variations and with consequent increased thermal stresses in the blade wall. It has to be pointed out that the thermal load enforced by the gas stream is mainly limited to the blade external walls (side walls) and therefore the partition between ducts may be considered as almost adiabatic.

Many studies, experimental as well as numerical have been made concerning the thermal behaviour of a fluid into 180deg turn static channels, amongst others Chyu [15], Lau et al. [16], Astarita et al. [17].

3.1. Experimental setup

A two-pass channel with four different aspect ratios AR (AR = 1, 2, 3 and 5) is presently tested; the channel cross section is $80mm$ (or 40, or 26.67, or $16mm$) high, $80mm$ wide and $2000mm$ long before and after the turn; these dimensions ensure a hydrodynamically fully developed flow ahead of the 180deg turn. The central partition wall between the two adjacent ducts is $16mm$ thick and ends with a square tip which is $80mm$ distant from the short side of the channel.

Two Pt100 RTD's measure the temperature at the entrance and at the outlet of the channel so as to monitor the overall temperature increase of air. The channel walls are manufactured from $16mm$ thick soft wood (to have a low thermal conductivity) but, towards the turn zone for a length of about $1200mm$, each one of the two channel side walls is realised with three printed circuit boards ($400mm$ long each) which are connected in series. It is therefore possible to have two different heating boundary conditions, in particular: heating from one side (asymmetrical), or two sides (symmetrical). The printed circuits are designed so as to achieve a constant heat flux over the surface (except beneath the partition wall) by the Joule effect. Their tracks are $17\mu m$ thick, $3mm$ wide and placed at $3.2mm$ pitches; the overall thickness of each boards is $0.53mm$. A stabilised DC power source supplies the electric current to the circuits and the power input is monitored by precisely measuring voltage drop and current across them.

The air flowing in the channel is thus heated from printed circuit board side walls. The heat transfer coefficient is calculated by means of Eq.(1) where $T_{aw}=T_b$. In this case T_b is the stream bulk temperature which is evaluated by measuring the stagnation temperature at the channel entrance and by making a one-dimensional energy balance along the channel. Data is reduced in non-dimensional form in terms of the Nusselt number Nu. It has to be stressed that temperature, and consequently Nu, values very close to the side walls are not reliable since the latter, which are bonded to the printed circuit board and are not heated, tend to behave like fins.

In the present paper, experimental measurements are carried out by means of AGEMA Thermovision 900LW infrared system. The field of view (which depends on the optics focal length and on the viewing distance) is scanned by the Hg-Cd-Te detector in the 8-12μm infrared window. Nominal sensitivity, expressed in terms of noise equivalent temperature difference, is $0.07°C$ when the scanned object is at ambient temperature. The scanner spatial resolution is 235 instantaneous fields of view per line at 50% slit response function. Each image is digitised in a frame of 136×272 *pixels* at 12 bit. An application software is used, which generally involves for each thermal image noise reduction by numerical filtering, computation of temperature, evaluation of radiation and tangential conduction losses and heat transfer correlation. The surface viewed by IR camera is coated with a thin film of black opaque paint with emissivity factor ε equal to 0.95.

Present data are corrected for both radiation heat transfer losses and non isotropic tangential conduction within the printed circuit board. Corrections because of the presence of natural convection from the viewed bottom surface of one of the heated walls are also considered.

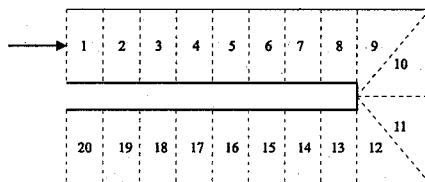Both the Nusselt number and the Reynolds number are based on the hydraulic diameter of the channel d.

Fig. 1. Measurement zones

In order to compare the experimental results with those of the literature, the Nusselt number is normalised by means of the classical Dittus and Boelter correlation for fully developed flow:

$$Nu^* = 0.024 \cdot Re^{0.8} \cdot Pr^{0.4} \tag{3}$$

It has to be pointed out that the use of the Dittus and Boelter correlation in the case of gases induce, an overestimate that may reach up to 20% of the real value.

An error analysis, based on the calibration accuracy of the infrared system and repeatability of measurements, indicates that heat transfer measurements are accurate to within about ±3.5%.

3.2. Results

In order to compare them with existling literature data, the experimental results are presented in terms of averaged Nusselt number profiles and the measurement domain corresponds to one third of the whole heated zone nearby the turn. Averages are made on each of the 20 zones shown in Fig. 1. The first eight rectangular zones, corresponding to the channel inlet, are half channel width long and one width wide; the following four ones of triangular shape correspond to the turn zone; the last eight zones of the same geometry of the first eight zones correspond to the channel outlet.

In Fig. 2 the segment by segment averaged Nusselt number profiles for an aspect ratio AR=1, different Re values and for the two tested boundary conditions, i.e. one or two heated walls, are shown. By examining the figure the following observations can be made:

- for all the different conditions a fully developed flow is reached before the inlet, in fact the Nusselt number is practically constant in the first seven zones, the Nu values being lower than those predicted by the Dittus and Boelter correlation;
- at the eighth region, i.e. about half hydraulic diameter before the turn, the Nusselt number begins to rise; in particular, at the end of the turn, it can reach a maximum value which is five times higher than that corresponding to the fully developed flow;
- for all the tested Reynolds numbers and for both the boundary conditions, the highest heat transfer zone is the twelfth one, i.e. the second half of the second corner;
- just after this region the local heat transfer minimum is to be ascribed to the influence of the low heat transfer zone due to the separation bubble which is present downstream of the turning zone;
- the local maximum in the regions 15-16 tends to slightly move downstream for increasing Re; this shift is most probably due to the movement of a high heat transfer zone which is present near the partition wall;
- the local variations of the Nusselt number increase for the Reynolds number decreasing;
- the two different heating conditions do not influence significantly the Nusselt number in the inlet channel; further downstream, the curves, relative to heating from both sides, are systematically placed above those relative to heating from one side only;
- the curve shape does not appear to be influenced by the thermal boundary condition;
- within the measurement region a completely redeveloped flow is not yet recovered.
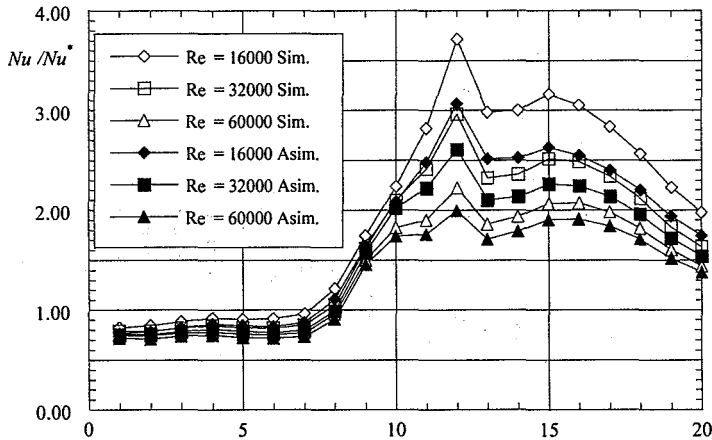
Fig. 2. Segment by segment normalised Nusselt number for *AR*=1

The comparison of the present measurements with those of Han et al. [18] is quite satisfactory; there is only a small difference in the maximum heat transfer value which may be partially ascribed to the different ratio between the width of the channel and that of the partition wall (5 in the present work and 4 in that of Han et al. [18]).

The segment by segment Nusselt profiles for an aspect ratio of 2 and for testing conditions equal to those of the previous figure are shown in Fig. 3. It is possible to note some differences as well as some analogies with the case of *AR*=1:

- as in the previous case, a completely developed flow is reached at the inlet of the channel and the normalised Nusselt number value is significantly lower than unity;
- the twelfth zone, which for *AR*=1 is an absolute maximum, becomes only a local maximum for the two higher *Re* values;
- the maximum increase of the Nusselt number is significantly lower with respect to the case of *AR*=1;
- as in the previous case, just after the twelfth zone, the influence of the separation bubble produces a local minimum in the convective heat transfer coefficient;
- the different boundary conditions have a more consistent influence on the convective heat transfer coefficient; in fact, even in the inlet channel, it is clearly visible that the curves for symmetrical heating are always above the corresponding ones for the asymmetrical condition;
- in the turn zone and for the lower Reynolds number, the Nusselt number for symmetrical heating is about 25% higher than that for the asymmetrical case.

4. Heat transfer to air from a yawed circular cylinder

The study of the velocity field and of the surface heat transfer of bodies exhibiting regions of separated flow is of great interest from both the scientific and practical points of view. In particular, cylindrical bodies with circular cross-section placed in a longitudinal flow are found in many engineering applications; the flow field around them is characterized by different types and extent of flow separation and reattachment according to the geometry of the cylinder upstream end and to the angle of attack of their axis relative to the incoming flow.
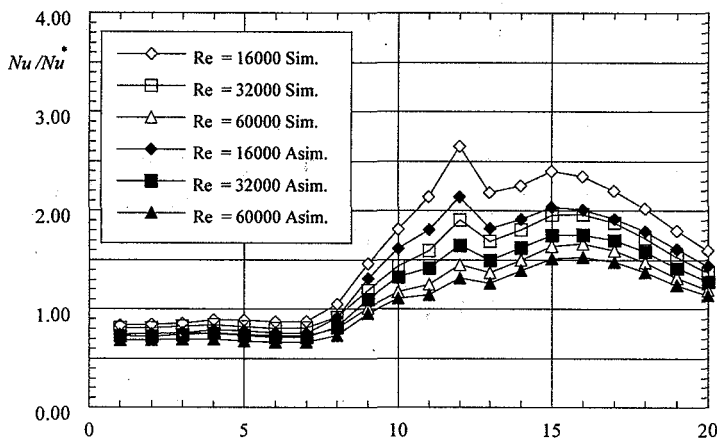
Fig. 3. Segment by segment normalised Nusselt number for *AR*=2

The flow field and surface heat transfer characteristics of a sharp-edged circular cylinder immersed in a stream at zero angle of attack α are the subject of a number of previous investigations. *Ota* [19], from experiments carried out for the Reynolds number *Re* (based on the cylinder diameter) ranging from 24,900 to 53,600, finds that the reattachment point of the bubble originating at the front sharp leading edge occurs at 1.6 diameters from the latter (*x/D* = 1.6); he derives this value as the mean of measurements obtained by exploiting three different techniques (tuft exploration, zero skin friction and nearly maximum pressure). However, in a subsequent paper concerning heat transfer measurements (*Ota and Kon* [20]), it is argued that the flow reattachment occurs at the position where a maximum is attained for the heat transfer coefficient, i.e. at *x/D* = 1.3. Actually, the authors report the value 1.4 but *Sparrow et al.* [21] notice that the effective maximum occurs at *x/D* = 1.3. For similar Reynolds numbers, the same position for the heat transfer maximum is found by *Sparrow et al.* [21], who however demonstrate through surface visualizations that the real flow reattachment occurs further downstream, and in particular at *x/D* = 1.6 for the same flow conditions; in addition, they find that the values of both the locations at which flow reattachment and maximum heat transfer occur, decrease for Reynolds number decreasing below the value of 30,000. It should be mentioned that the free-stream turbulence intensity is 0.4 - 0.5 % in the tests of Sparrow et al., while it is approximately 0.8 % in the tests of Ota.

Conversely, no systematic study of the evolution of the flow field, or of the surface heat transfer, seems to be available for sharp-edged cylinders at an angle of attack. Nevertheless, it is reasonable to expect that the separation imposed by the front sharp edge may lead to an extended range of α for which a separation bubble is still present in the vicinity of the leading edge, and that the subsequent development of the flow is also in this situation more complex than in the case of zero angle of attack.

In the present paper heat transfer measurements on a circular cylinder at angles of attack varying from zero to 20° and for Reynolds numbers that extend the range of available data are performed by means of infrared thermography. The cylinder has either a flat sharp-edged or a hemispherical forebody attached to it.

4.1. Experimental setup

The experiments are carried out in the subsonic wind-tunnel of the Department of Aerospace Engineering of Pisa University, which is a closed-return Göttingen type wind tunnel with an open circular test section, 1.1*m* in diameter and 1.5*m* in length, and with free-stream turbulence of approximately 0.9 %.

The experiments are performed within the range 84,700 < Re < 159,000, with a test cylinder having a diameter of 80mm and an overall length of 1100mm. The model is supported at its back end by means of a sting, fastened to a special rig that allows the angle of attack to be varied continuously from - 25° to + 25°. Furthermore, in order to avoid any appreciable vibration of the cylinder, four thin steel wires connect a section of the model, aft of the measuring region, to a rigid frame positioned out of the wind-tunnel test section. Two different blunt forebodies may be attached to the cylinder: a flat sharp-edged disk or a hemispherical nose having a radius of curvature equal to 40mm.

The model surface is made out of a printed circuit board so as to produce, by Joule effect, a *constant* heat flux over it. The thickness and width of the copper conducting tracks of the circuit, which are aligned with the cylinder axis, are manufactured with very close tolerances; in detail, the tracks are 35μm thick, 4.5mm wide and placed at 5.0mm pitch. The heated zone of the cylinder (i.e. the length of the copper tracks) is 600mm long and starts 10mm downstream of the sharp leading edge. The board (which constitutes the cylinder wall exposed to the free stream) has an overall thickness of about 1mm, with the conducting tracks plunged 0.2mm below its external surface, and is in contact with a thick layer of thermal insulation which is placed inside it. A stabilized DC power source supplies the electric current to the circuit and the power input is monitored by precisely measuring voltage drop and current across it.

The model surface, which is viewed by the infrared camera, is coated with a thin layer of black paint that has a directional emissivity coefficient equal to 0.95 in the wavelengths of interest and for viewing angles comprised between 40° and 90°; the data corresponding to viewing angles lower than 40° are not herein considered since the directional emissivity coefficient of the surface decreases rapidly below this value.

The infrared camera measures the distribution of the wall temperature T_w of portions of the heated surface. The wall temperature is correlated to the heat transfer coefficient by means of the steady state *heated-thin-foil* technique (described in paragraph 2).

The heat transfer coefficients are evaluated in non-dimensional form by means of the local Nusselt number based on the cylinder diameter D (the thermal conductivity coefficient of air evaluated at film temperature).

The employed infrared thermographic system is the AGEMA Thermovision 880. The field of view (which depends on the optical focal length and on the viewing distance) is scanned by the Hg-Cd-Te detector in the 8-12μm infrared window. The nominal sensitivity, expressed in terms of noise equivalent temperature difference, is 0.07°C when the scanned object is at ambient temperature. The scanner spatial resolution is 175 instantaneous fields of view per line at 50% slit response function. A 20° lens is used during the tests at a viewing distance of 2m, which gives a field of view of about 0.3 x 0.3m^2; this is done to obtain a higher spatial resolution in the thermal image. Therefore, in order to measure temperatures in the whole heated zone and to account for the directional emissivity coefficient, six different thermal images (two in the longitudinal direction times three in the azimuthal one) are taken and *patched up*. Each image is digitized at 8 bits in a frame of 140 x 140 pixels. An application software can perform: patching of images, identification of the measured points on the cylinder surface, noise reduction by numerical filtering, computation of temperature and heat transfer correlations.

An error analysis, based on the calibration accuracy of the infrared system and repeatibility of measurements, indicates that heat transfer measurements are accurate to within about ±5%.
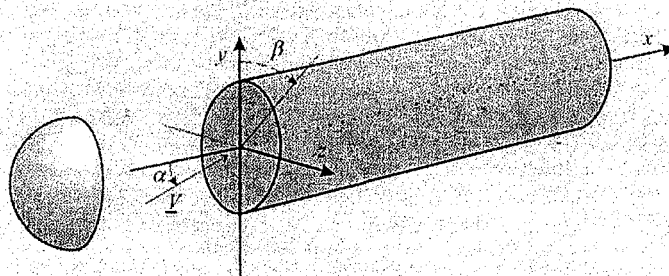
Fig. 4. Fluid Flow configuration and coordinate axes

4.2. Results

The fluid flow configuration and the coordinate axes used for the description of the results are schematically shown in *Fig. 4*. It should be noted that the position $x = 0$ corresponds to the start of the cylindrical part of the body, so that it coincides with the leading edge of the flat sharp-edged model, and with the end of the forebody in the case of the model with a hemispherical nose (which thus originates at $x/D = -0.5$). The azimuthal coordinate β starts at the leeward generating line. Furthermore, it has to be pointed out that, due to the effective position of the heating and to the strong end-conduction effects near the forebody and the afterbody, the portion of the cylinder for which the infrared camera gives reducible data actually starts at $x/D = 0.25$ and ends at $x/D = 7.5$.

A comparison between the results obtained in the present investigation for the sharp-edged cylinder (at zero angle of attack and for the three different Reynolds number values) and those obtained by *Ota and Kon* [20] is shown in *Fig. 5*. The whole data is reported in terms of the parameter $Nu/Re^{0.75}$ already used by Ota and Kon which, as it can be seen from the figure, allows a good coalescence of all the present measurements. The axial distribution of this parameter is characterized by an initial increase, a local maximum, which is located at approximately $x/D = 1.2$, and a subsequent monotonic decrease corresponding to a redeveloping flow. The initial low heat transfer region corresponds to the separated flow which is present just downstream of the cylinder nose. It must be remembered that the location of the maximum convective heat transfer does not exactly coincide with that of flow reattachment, which is located slightly downstream of this position (*Sparrow et al.,* [21]).

As can be seen from *Fig. 5*, the position of the maxima and their values are in all cases relatively consistent with the findings of *Ota and Kon* [20] that are also shown in the figure, as well as with the data (not shown in *Fig. 5*) of *Sparrow et al.* [21] for $Re > 30,000$, notwithstanding the different ranges of Re. The present data shows a sharper peak with respect to that of Ota and Kon; this difference may be most certainly ascribed to the fact that Ota and Kon seem to ignore tangential conduction effects in their relatively thick walled model.

In *Figs. 6* to *9* the evolution of the isocontours of the dimensionless surface heat transfer coefficient $Nu/Re^{0.75}$ is shown in the case of the sharp-edged model at four increasing angles

of attack for Re = 119.000. To highlight the surface flow features, the dimensions of the cylinder are not shown to scale; in fact the represented cylinder length is equivalent to 7.25 D and, as already mentioned, it starts at 0.25 D from the leading edge. The different values of the parameter $Nu/Re^{0.75}$ may be derived from the colour scale attached to the figures, which also show the position of the windward generating line corresponding to β =180°.
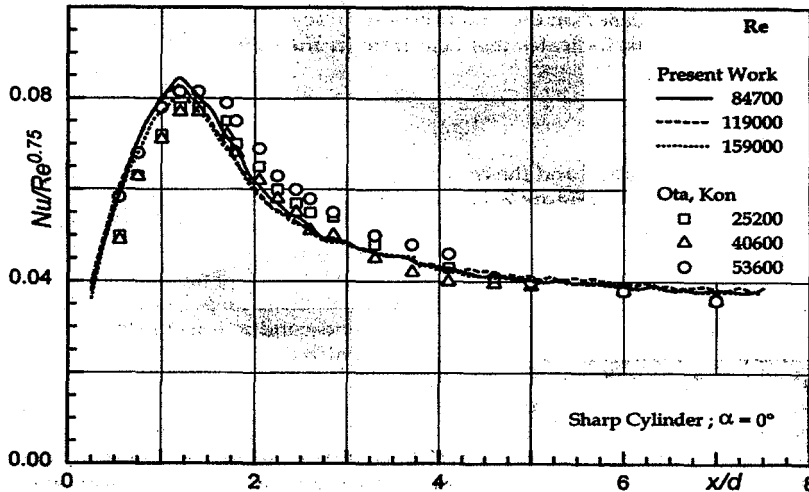

Fig. 5. Distribution of $Nu/Re^{0.75}$ on the sharp edge cylinder at α=0° for various Reynolds numbers

From *Figs. 6-9* it can be noticed that, as α increases, the heat transfer surface pattern becomes progressively more two-dimensional. In particular, it is clear that the shape of the separation bubble, whose presence may still be recognized at the lower angles of attack, changes with a strong reduction of its length on the windward side and a slight increase on the leeward side. Furthermore, inside the bubble the intensity of the heat transfer varies azimuthally, with a significant decrease in the upper region (i.e. towards $\beta = 0°$) with respect to the case of $\alpha = 0°$. This feature is probably a consequence of the reduction of the friction coefficient connected with the coalescence of the limit streamlines towards the leeward generating line in the plane of symmetry that becomes a *local line of separation*. For $\alpha = 20°$, the highest heat transfer zones are reduced to two small spots located in the vicinity of $\beta \cong 90°$ at the beginning of the measured region and, by extrapolating upstream the heat transfer map, the separation bubble at $\beta = 180°$ (windward generating line) seems to disappear.

Another feature that can be derived from *Figs. 6 - 9* is the progressive appearance, on the cylinder sides, of a low heat transfer region, which starts in the aft end of the image at $\alpha = 5°$, and moves upstream with increasing angle of attack, simultaneously becoming sharper, and seemingly enhancing the global three-dimensionality of the flow. This region is presumably connected with the fact that the increasingly intense cross-flow leads first to instabilities of the boundary layer, and eventually to the separation from the sides of the cylinder of dominating longitudinal vortical structures. Within the heated region, the azimuthal location of the detected minimum heat transfer coefficient varies from $\beta \cong 70°$ for $\alpha = 5°$; to $\beta \cong 55°$ for $\alpha = 10°$ and 15°; to $\beta \cong 75°$ for $\alpha = 20°$.

By comparing the maps of Nusselt number (not shown herein) in the case of the cylinder with a hemispherical forebody the with the ones of *Figs. 6-9* it is possible to notice that the change from the sharp-edged forebody to the hemispherical one causes significant

differences to occur, from both the qualitative and the quantitative points of view. Indeed, the overall heat transfer is lower than for the sharp-edged cylinder at corresponding angles of attack and the separation bubble now seems to be either absent or extremely reduced in size, and in any case presumably positioned immediately before the zone viewed by the infrared camera.

The influence of the leading edge on the surface heat transfer, and consequently on the flow field, is much more confined to the initial region of the cylinder. Furthermore, there is a much more rapid progression of the surface pattern, and consequently of the flow features, with increasing angle of attack. Then, the conclusion can be drawn that in the case of the sharp-edged cylinder the persistence and considerable extent of the front separation bubble inevitably produces a downstream movement of the longitudinal vortices separating from the sides of the cylinder at high angles of attack, whereas with the smoother hemispherical forebody the detachment of these vortices occurs more upstream for the same values of α, moving rapidly to a position just behind the start of the cylindrical region of the model. This behavior is also clearly shown by the almost constant (in the x direction) heat transfer coefficient on the leeward side of the round-nosed cylinder aft part. All the above described findings show a more upstream located attainment of a quasi-two-dimensional flow field, typical of cylinders in cross flow, in the case of the cylinder with a hemispherical nose.

5. Conclusion

Infrared thermography applied to the *heated-thin-foil* tecnhique has been used to measure convective heat transfer coefficients in static 180deg turn channels and over a yawed circular cylinder immersed in air stream.

The thermal behaviour of the fluid through the static channel is analysed segment by segment, starting from the inlet where a fully developed flow is reached for all the tested conditions. It has been found that the Nusselt number, initially constant, begins to rise, at about the half hydraulic diameter before the turn, and reaches its maximum value at about the second half of the second corner; a local minimum heat transfer zone is encountered, which is due to the separation bubble located downstream of the turning zone. After, the Nu value increases again due to the impinging flow on the partition wall before exhaust. In general, Nu/Nu^* value increases as the Reynolds number decreases. An increase in the aspect ratio entails a decrease in the average heat transfer coefficients; the peaks become much milder and the Nu values are much more sensitive to the heating conditions (symmetrical or asymmetrical).

The results for the sharp-edged cylinder at $\alpha = 0°$ show a one-dimensional distribution of the Nusselt number on the cylinder surface that is generally consistent with previous data obtained by other authors for lower values of the Reynolds number. In particular the presence of a leading edge *thermal* separation bubble may be recognized, its length being determined by the position of the maximum heat transfer coefficient. When the angle of attack is increased, this bubble still seems to be present, but changes considerably in shape with a moderate increase of its length on the leeward side and a substantial decrease on the windward side. Conversely, the cylinder with the hemispherical nose is characterized by a decrease of the three-dimensionality of the flow in the body front region with respect to the previous case and probably by a much smaller separation bubble, positioned upstream of the measured region. The most significant difference is that a quasi-two-dimensional flow field around the cylinder is attained more upstream in the case of the cylinder with a hemispherical forebody.

Results prove that the infrared radiometer is a powerful tool; however, precise quantitative measurements require that all the potential error sources and modulations should be reduced and the most appropriate testing procedure to the specific flow configuration adopted.

REFERENCES

[1] CARLOMAGNO (G. M.) and DE LUCA (L.) - *Infrared Thermography in Heat Transfer, Handbook of Flow Visualization*, (ed. W.J. Yang) chap. 32, Hemisphere, 1989, pp. 531-553.

[2] CARLOMAGNO (G. M.) - *Heat Transfer Measurements by means of Infrared Thermography, in Measurement Techniques*, von Karman Institute for Fluid Mechanics Lect. Series 1993-05, Rhode-Saint-Genese, 1993, pp. 1-114.

[3] SIMEONIDES (G.), D. VAN LIERDE (P.), VAN DER STICHELE (S.), CAPRIOTTI and WENDT (J. F.) - *Infrared Thermography in Blowdown and Intermittent Hypersonic Facilities*, AIAA Paper 89-0042, 1989.

[4] HENCKELS (A.), MAURER (F.), OLIVIER (H.) and GRÖNIG (H.) - *Fast Temperature Measurement by Infrared Line Scanning in a Hypersonic Shock Tunnel*, Experiments in Fluids, Vol. 9, 1990, pp. 298-300.

[5] CARDONE (G.), ASTARITA (T.) and CARLOMAGNO (G. M.) - *Infrared Thermography to Measure Local Heat Transfer Coefficients on a Disk Rotating in Still Air*, Proceedings of the Workshop Advanced Infrared Technology and Applications, Baccini & Baldi, Firenze, 1996, pp. 143-153.

[6] CARLOMAGNO (G. M.) and DE LUCA (L.) - *Heat Transfer to Impinging Jets Measured by Infrared Thermography*, Proc. COBEM 89 (eds. M. H. Hirata et al.), Rio de Janeiro, 1989, pp.209-212.

[7] DE LUCA (L.), CARLOMAGNO (G. M.) and BURESTI (G.) - *Boundary Layer Diagnostics by Means of an Infrared Scanning Radiometer*, Experiments in Fluids, Vol. 9, 1990, pp.121-128.

[8] CARDONE (G.) and CARLOMAGNO (G. M.) - *Convezione naturale su lastra piana nei regimi stazionario ed instazionario*, Atti IX Congresso Nazionale UIT, Pisa, 1991, pp. 397-410.

[9] HEATH (D. M.), WINFREE (W. P.), CARRAWAY (D. L.) and HEYMAN (J. S.) - *Remote Noncontacting Measurements of Heat Transfer Coefficients for Detection of Boundary Layer Transition in Wind Tunnel Tests*, Proc. 12th Int. Congr. Instrumentation Aerospace Simulation Facilities, Williamsburg , 1987, pp. 135-140.

[10] BALAGEAS (D. L.), BOSCHER (D. M.), DÈOM (A. A.), FOURNIER (J.) and GARDETTE (G.) - *Measurement of Convective Heat Transfer Coefficients in Wind Tunnels using Passive and Stimulated Infrared thermography*, Rech. Aerosp., 1991-4, pp.51-72.

[11] CARLOMAGNO (G. M.), DE LUCA (L.) and ALZIARY DE ROQUEFORT (T.) - *Mapping and Measurement of Aerodynamic Heating and Surface Flow Visualization by means of IR Thermography*, in Multiphase Flow and Heat Transfer, (Eds. Chen et al.), Vol. 2, Hemisphere, 1991, pp. 1316-1324.

[12] BYNUM (D. S.), HUBE (F. K.), KEY (C. M.) and DIEK (P. M.) - *Measurement and Mapping of Aerodynamic Heating with an Infrared Camera*, AEDC Rept. TR-76-54, 1976, pp. 1-33.

[13] DE LUCA (L.), CARDONE (G.), CARLOMAGNO (G. M.), AYMER DE LA CHEVALERIE (D.) and ALZIARY DE ROQUEFORT (T.) - *Flow Visualization and Heat Transfer Measurement in a Hypersonic Wind Tunnel*, Experimental Heat Transfer, Vol. 5, 1992, pp. 65-78.

[14] CARLOMAGNO (G. M.) - *Thermo-fluid-dynamic applications of Quantitative infrared thermography,* Int. J. of Flow Visualisation and image processing, Vol. 4, 1998 pp. 261-280.

[15] CHYU (M. K.) - Regional Heat Transfer in Two–Pass and Three–Pass Passages With 180–deg Sharp Turns, J. Heat Transfer, Vol. 113, 1991, pp. 63–70.

[16] LAU (S. C.), RUSSEL (L. M.), THURMAN (D. R.) and HIPPENSTEELE - *Visualization of Local Heat Transfer in Serpentine Channels with Liquid Crystals*, Proc. V Int. Symp. On Transport Phenomena and Dynamics of Rotating Machinery, Kaanapaly, Hawaii, 1994, Vol. A, pp. 411–423.

[17] ASTARITA (T.), CARDONE (G.) and CARLOMAGNO (G. M.) - *Average Heat Transfer Measurements Near a Sharp 180° Turn Channel for Different Aspect Ratios*, Optical Methods and Data Processing in Heat and Fluid Flow, IMechE Conf. Trans., London 1998, pp137-146.

[18] HAN (J. C.), ZHANG (Y. M.), KALKUELHLER (K.) - *Uneven Wall Temperature Effect on Local Heat Transfer in a Rotating Two-Pass Square Channel with Smooth Walls*, ASME Journal of Heat Transfer, 1993, Vol. 114, pp. 850-858.

[19] OTA (T.) - An Axisymmetric Separated and Reattached Flow on a Longitudinal Blunt Circular Cylinder, J. Applied Mech., Vol. 42, pp.311-315, 1975.

[20] OTA (T.), KON (N.) - Heat Transfer in an Axisymmetric Separated and Reattached Flow Over a Longitudinal Blunt Circular Cylinder, J. Heat Transfer, Vol. 99, pp. 155-157, 1977.

[21] SPARROW (E. M.), KANG (S. S.), CHUCK (W.) - *Relation Between the Points of Flow Reattachment and Maximum Heat Transfer for Regions of Flow Separation*, Int. J. Heat Mass Transfer, Vol. 30, pp. 1237-1246, 1987.
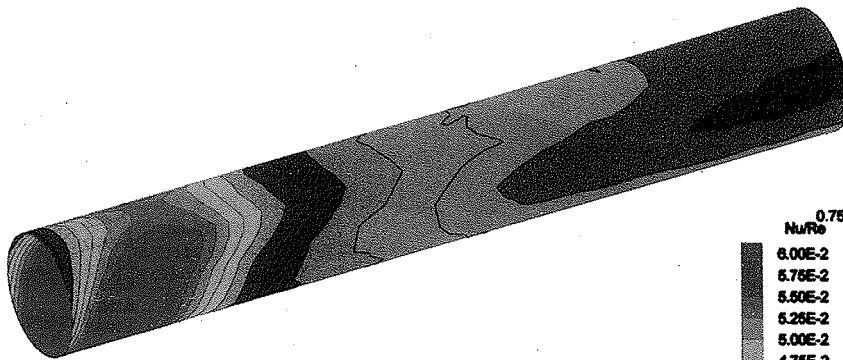
Sharp-edged Cylinder
Re = 119000
α = 5°

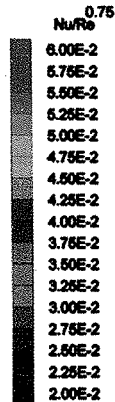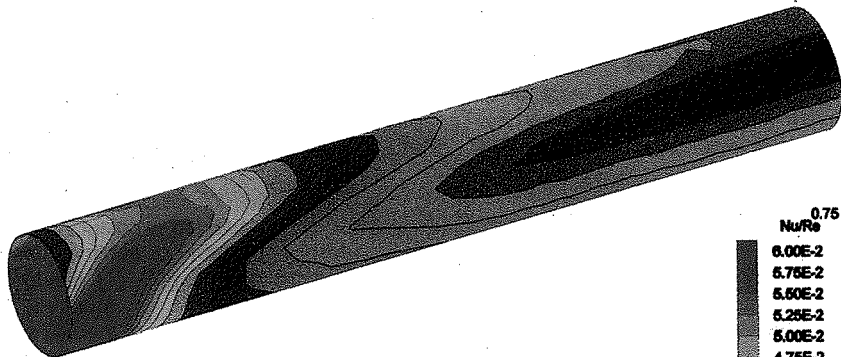Fig. 6. Isocontours of Nu/Re$^{0.75}$ on the sharp-edged cylinder at α = 5°, Re = 119,000

Sharp-edged Cylinder
Re = 119000
α = 10°

Fig. 7. Isocontours of Nu/Re$^{0.75}$ on the sharp-edged cylinder at α = 10°, Re = 119,000

Sharp-edged Cylinder
Re = 119000
$\alpha = 15°$

$$\frac{Nu}{Re^{0.75}}$$

6.00E-2
5.75E-2
5.50E-2
5.25E-2
5.00E-2
4.75E-2
4.50E-2
4.25E-2
4.00E-2
3.75E-2
3.50E-2
3.25E-2
3.00E-2
2.75E-2
2.50E-2
2.25E-2
2.00E-2

Fig. 8. Isocontours Nu/Re$^{0.75}$ on the sharp-edged cylinder at α = 15°, Re = 119,000

Sharp-edged Cylinder
Re = 119000
$\alpha = 20°$

$$\frac{Nu}{Re^{0.75}}$$
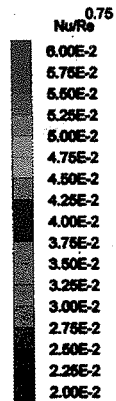
6.00E-2
5.75E-2
5.50E-2
5.25E-2
5.00E-2
4.75E-2
4.50E-2
4.25E-2
4.00E-2
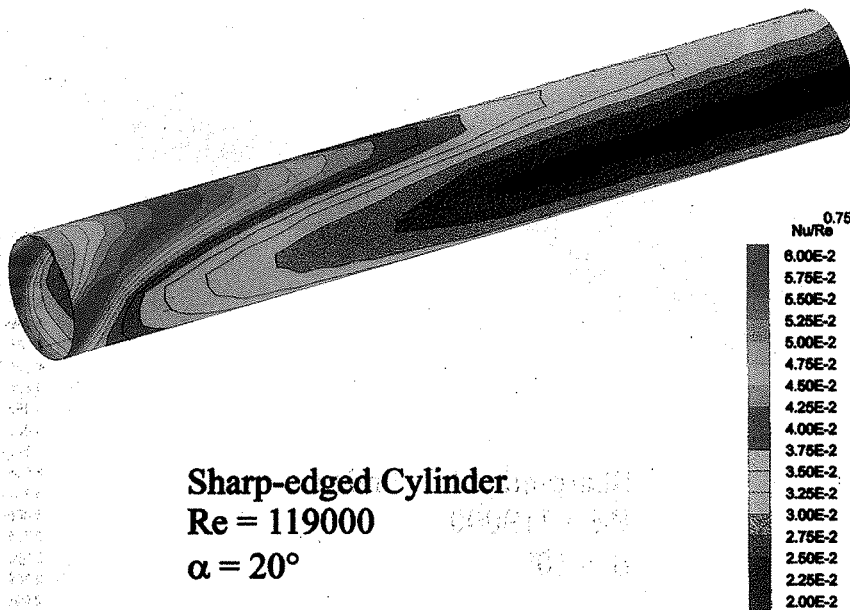3.75E-2
3.50E-2
3.25E-2
3.00E-2
2.75E-2
2.50E-2
2.25E-2
2.00E-2

Fig. 9. Isocontours Nu/Re$^{0.75}$ on the sharp-edged cylinder at α = 20°, Re = 119,000